Relating Interfacial Order to Sum Frequency Generation with Ab-Initio Simulations of the Aqueous Al_2O_3 (0001) and (11$\bar{2}$0) Interfaces: Supplemental Information

Mark DelloStritto,[†,‡] Stefan Piontek,[†] Michael Klein,[†,¶,‡] and Eric Borguet[*,†,‡]

†*Department of Chemistry, Temple University, Philadelphia, Pennsylvania 19122, United States*

‡*Center for the Computational Design of Functional Layered Materials*

¶*Institute for Computational Molecular Science*

E-mail: eborguet@temple.edu

Radial Distribution Functions

In this section we plot the O-O Radial Distribution Functions (RDFs) for all O atoms in H_2O molecules for the $Al_2O_3(0001)$-H_2O and $Al_2O_3(11\bar{2}0)$-H_2O interfaces simulated using the PBE-TS and RPBE functionals. The RDFs have been scaled by the fraction of the cell occupied by H_2O molecules such that they go to unity at long distances. We plot the RDFs for the (0001) and $(11\bar{2}0)$ interfaces in Figure 1.

The PBE-TS simulations lead to a good description of the structure of water, with peak (locations,intensities) of (2.68Å,2.90) and (4.3Å,1.05) and a trough at (3.2Å,0.40) for the (0001) interface, and peaks at (2.7Å,2.65) and (4.32Å,1.10) and a trough at (3.2Å,0.5) for the $(11\bar{2}0)$ interface.

The RPBE simulations have much less ordered water, with peak (locations,intensities) of (2.76Å,2.2) and (4.0Å,1.0) and a trough at (3.25Å,0.8) for the (0001) interface. The simulations of the $(11\bar{2}0)$ interface have peak (locations,intensities) of (2.74Å2.8) and (4.16Å,1.2) and a trough at (3.2Å,0.76). While the O-O RDF for the RPBE functional is less structured than the RDF for the PBE-TS functional for each interface, the RDF for the $(11\bar{2}0)$ interface is slightly more structured than for the (0001) interface. This is likely because the RPBE simulation of the (0001) interface is less ordered and has shorter H-bond lifetimes than the RPBE simulation of the $(11\bar{2}0)$ interface, as detailed in the main text.

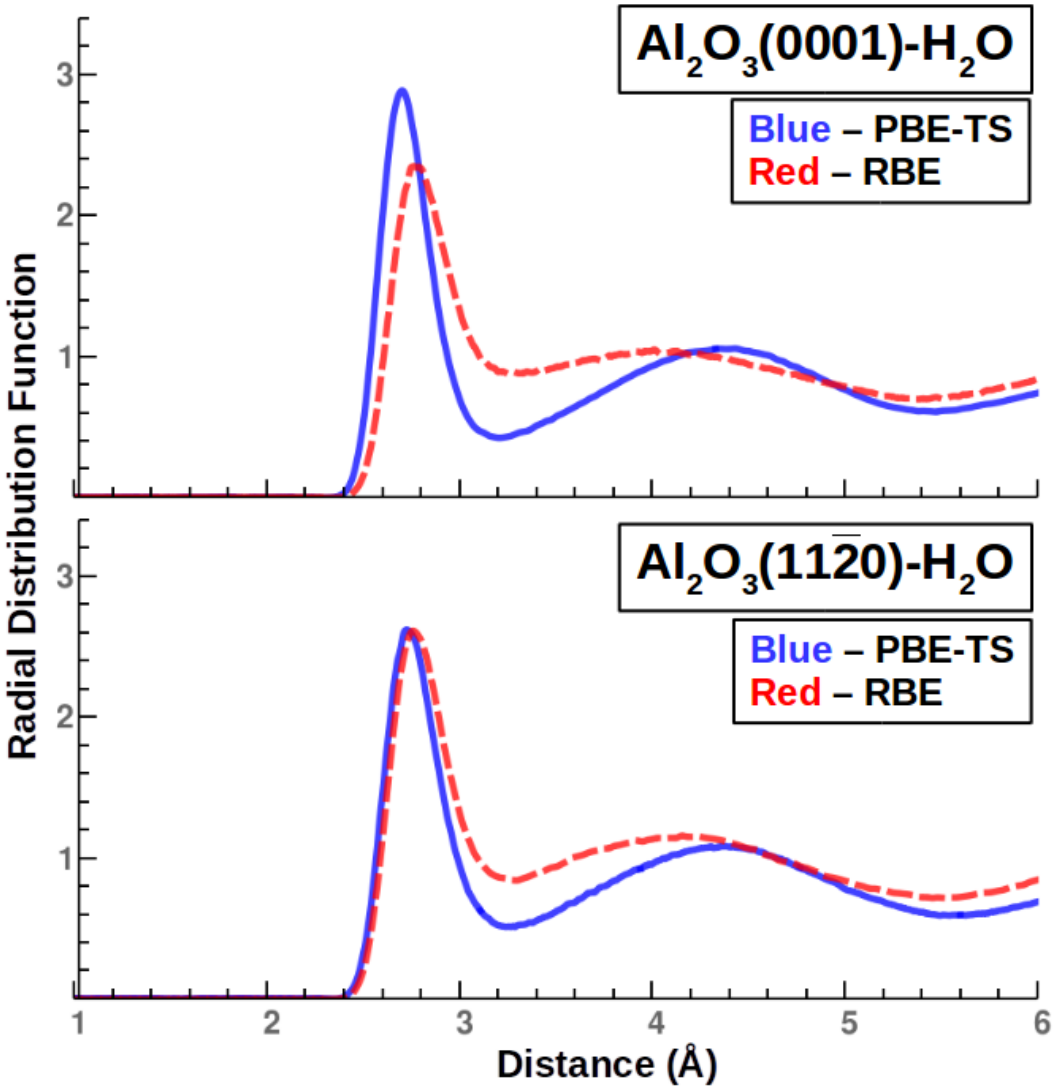

Figure 1: The O-O RDF for O atoms which are part of H_2O molecules at the $Al_2O_3(0001)$-H_2O and $Al_2O_3(11\bar{2}0)$-H_2O interfaces. For each inteface, The blue solid line is the average over the PBE-TS simulations, while the red dashed line is the average over the RBPE simulations.

Surface Structure

In this section we detail the structure of the alumina-water interfaces studied and compare them to X-Ray Reflectivity (XRR) measurements. In order to facilitate comparison between experimental and theoretical values, we normalize the experimental and calculated values by setting the bottom-most atom position to zero. All reported positions are in Å.

In Table 1 we list the average positions of the O and Al atoms in the oxide surface and the average position of the first O peak of the H_2O molecules for the $Al_2O_3(0001)$-H_2O interface simulated using the PBE-TS and RBPE functionals, with the absolute differences from experiment for each functional appearing the next column to the right. We compare to XRR measurements from Catalano.[1]

Table 1: $Al_2O_3(0001)$-H_2O Interfacial Structure (Å).

Atom	Expt.	PBE-TS	Diff	RPBE	Diff
O-H_2O	8.15	8.34	0.19	8.53	0.38
O	5.69	5.70	0.01	5.77	0.08
Al	4.74	4.80	0.06	4.85	0.11
Al	4.37	4.51	0.14	4.57	0.20
O	3.54	3.53	0.01	3.57	0.03
Al	2.72	2.67	-0.05	2.71	-0.01
Al	2.17	2.17	0.00	2.20	0.03
O	1.32	1.33	0.01	1.35	0.03
Al	0.51	0.48	-0.03	0.48	-0.03
Al	0.00	0.00	0.00	0.00	0.00

In Table 2 we list the average positions of the O and Al atoms in the oxide surface and the average position of the first O peak of the H_2O molecules for the $Al_2O_3(11\bar{2}0)$-H_2O interface simulated using the PBE-TS and RBPE functionals, with the absolute differences from experiment for each functional appearing the next column to the right. We compare to XRR measurements from Catalano.[2]

For both interfaces and both functionals the error in the positions of the interfacial atoms is rather small, typically on the order of 0.1 Å, with average errors around 1 Å. The largest errors for all interfaces occur for the position of the first and/or second peaks of the adsorbed

Table 2: $Al_2O_3(11\bar{2}0)$-H_2O Interfacial Structure (Å).

Atom	Expt.	PBE-TS	Diff	RPBE	Diff
O-H_2O	10.29	10.55	0.26	10.67	0.64
O-H_2O	8.97	9.19	0.22	9.48	0.51
O	7.58	7.44	-0.14	7.54	-0.04
O	7.39	7.20	-0.19	7.28	-0.11
O	6.83	6.66	-0.17	6.72	-0.11
O	6.64	6.47	-0.17	6.54	-0.10
Al	5.72	5.75	0.03	5.83	0.11
O	4.95	4.99	0.04	5.07	0.12
O	4.76	4.84	0.08	4.91	0.15
O	4.07	4.29	0.22	4.35	0.28
O	3.88	4.09	0.21	4.13	0.25
Al	3.30	3.34	0.04	3.39	0.09
O	2.57	2.61	0.04	2.65	0.08
O	2.38	2.41	0.03	2.43	0.05
O	1.77	1.86	0.09	1.89	0.12
O	1.58	1.68	0.10	1.70	0.12
Al	0.93	0.94	0.01	0.94	0.01
O	0.19	0.20	0.01	0.21	0.02
O	0.00	0.00	0.00	0.00	0.00

H_2O molecules, with errors around 0.2-0.4 Å. This is expected, partly because of systematic errors in the structure of water resulting from the use of GGA functionals, and partly because the XRR fitting for the H_2O peaks must rely on a simplified model of the structure factor interfacial water which may introduce small errors into the final positions. Either way, we believe that these results demonstrate that both the PBE-TS and RPBE functionals are able to accurately reproduce the average structure of both the $Al_2O_3(0001)$-H_2O and $Al_2O_3(11\bar{2}0)$-H_2O interfaces.

Additionally, for both interfaces we plot the angular distribution function (ADF) of the surface aluminols. We plot the aluminol ADFs for the (0001) interface and the $(11\bar{2}0)$ interface in Figure 2. We plot the distribution of the cosine of the angle with respect to the z-axis, such that -1 indicates an OH group anti-parallel to the surface normal, 0 indicates an OH group parallel to the surface normal, and 1 indicates an OH group parallel to the surface normal.

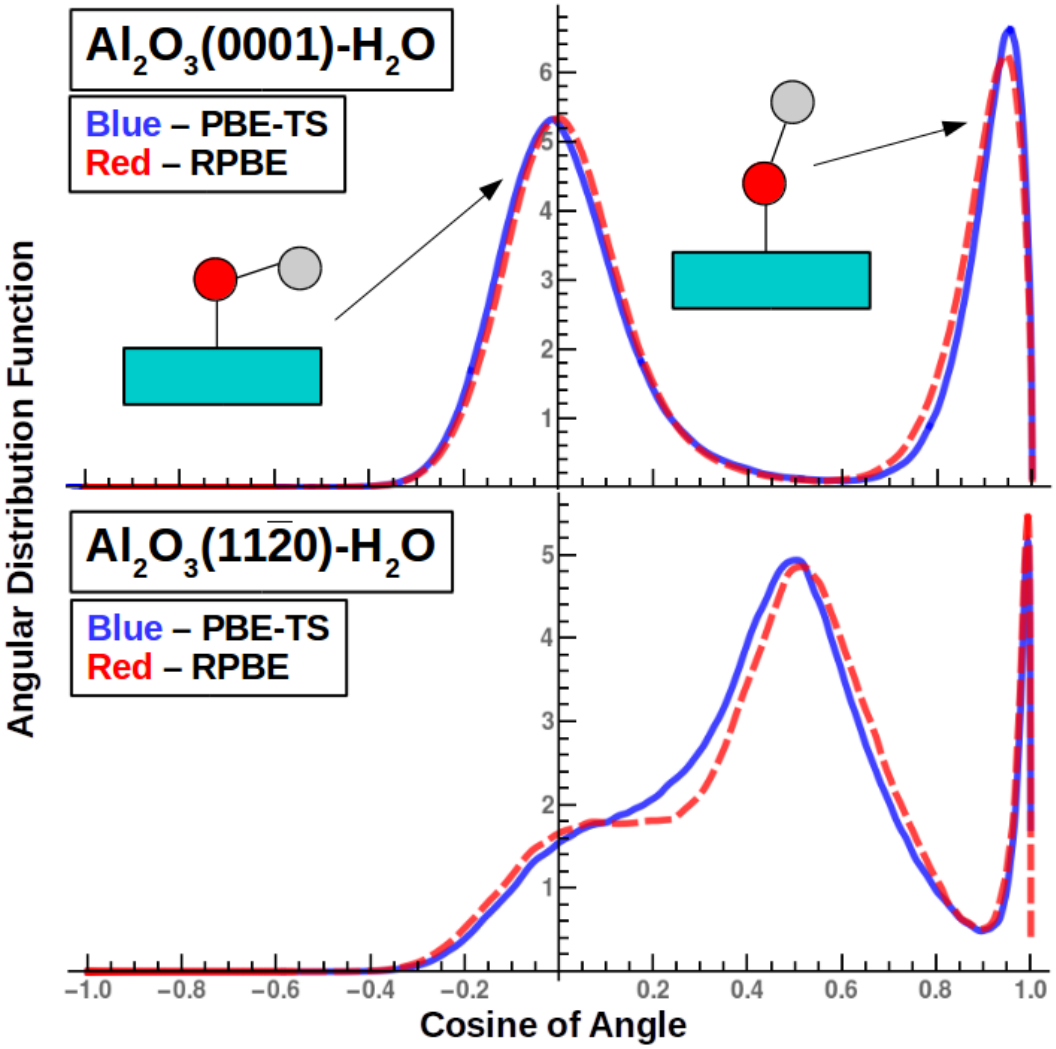

Figure 2: The ADFs of the surface aluminols at the (0001) and (11$\bar{2}$0) interfaces. In each plot, the solid blue line shows the ADF for the PBE-TS functional while the dashed red line shows the ADF for the RPBE functional.

Water Orientation

In Figure 3 we plot the ADF of the OH groups of the H_2O molecules not in the first layer of H_2O, where we see that there is little net orientation, as expected. In Figure 4 we plot the net dipole moment of the H_2O molecules, where again we see little net orientation beyond the first layer.

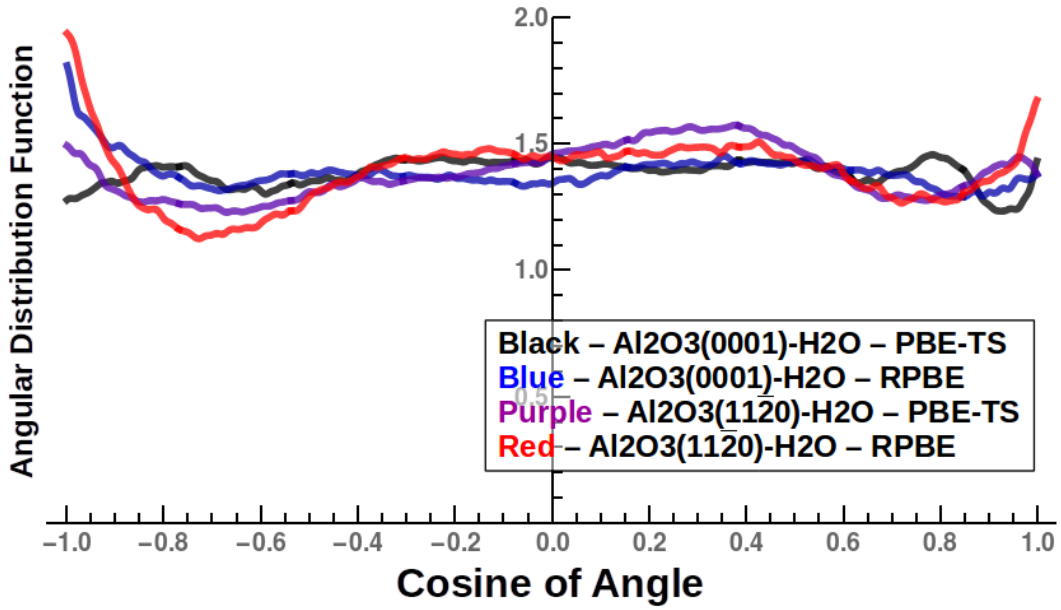

Figure 3: Angular distribution function of the H_2O molecules not in the first layer at the interface, averaged over each of the different simulations.

Density Profiles

In this section we plot the density profile of the heavy atoms (i.e. O and Al) for each of the interfaces and each of the functionals. Each of the density profiles are smoothed slightly using a Gaussian filter of width 4 bins (0.04 Å) and the heights of each of the elements are renormalized such that they have approximately the same maxima and can thereby be shown on the same plot.

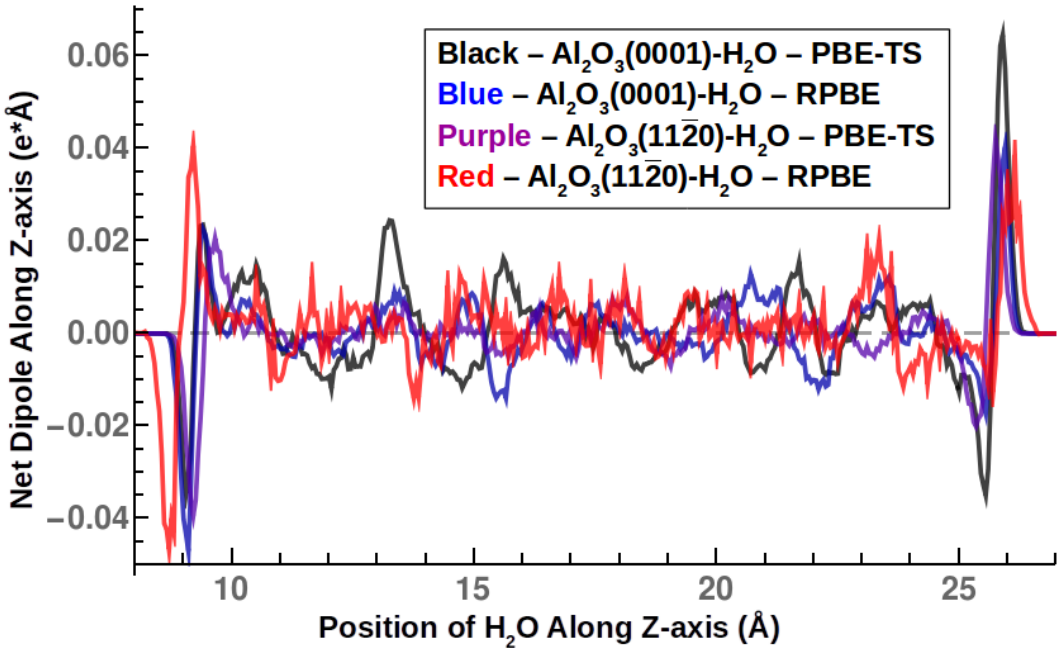

Figure 4: Net dipole moment of the H_2O molecules along the z-axis, averaged over each of the different simulations.

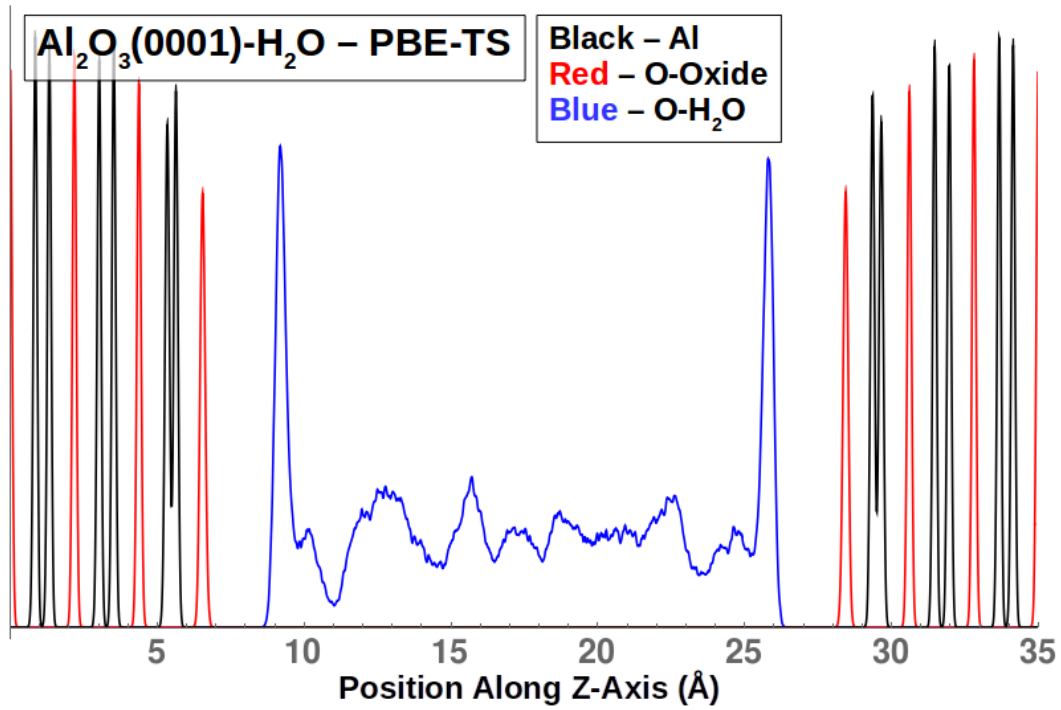

Figure 5: The density profile of the O and Al atoms for the (0001) interface simulated using the PBE-TS functional. The density profiles for the Al atoms, O atoms in the oxide, and O atoms in H_2O molecules are plotted using black, red, and blue lines, respectively. The profiles for the different elements have been rescaled to fit on the same vertical scale.

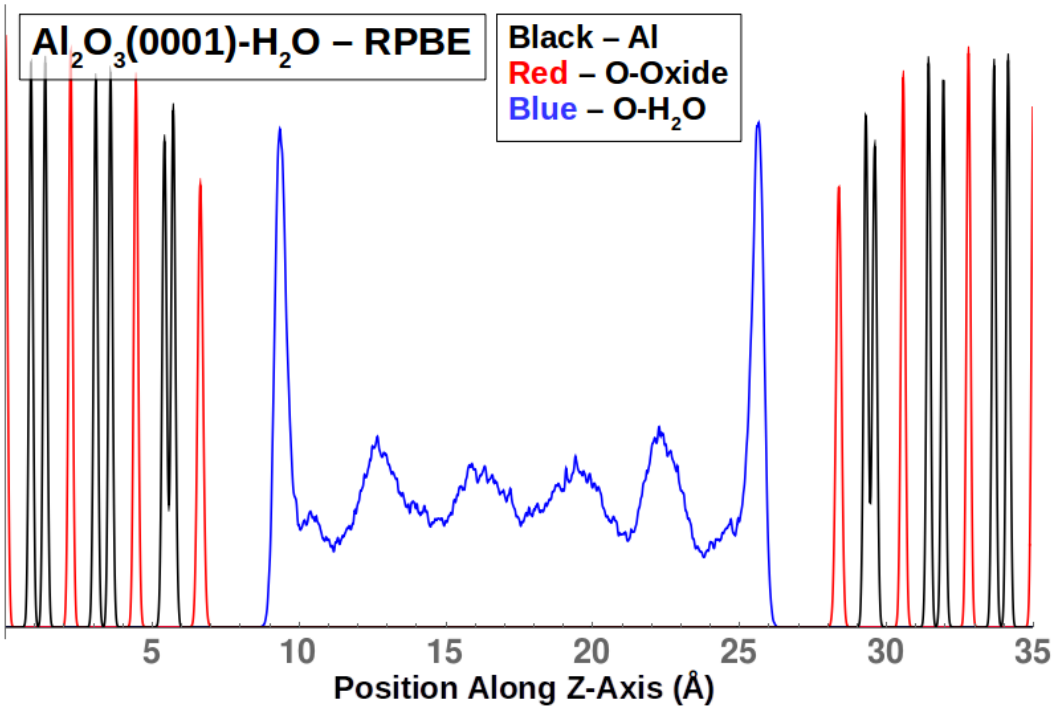

Figure 6: The density profile of the O and Al atoms for the (0001) interface simulated using the RPBE functional. The density profiles for the Al atoms, O atoms in the oxide, and O atoms in H_2O molecules are plotted using black, red, and blue lines, respectively. The profiles for the different elements have been rescaled to fit on the same vertical scale.

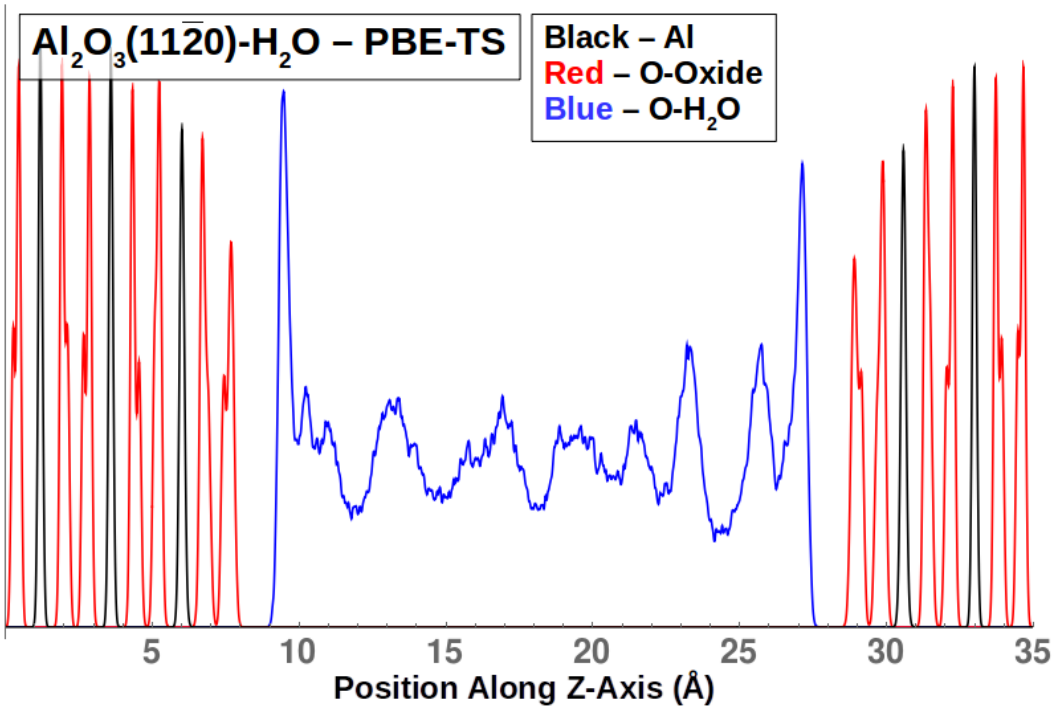

Figure 7: The density profile of the O and Al atoms for the $(11\bar{2}0)$ interface simulated using the PBE-TS functional. The density profiles for the Al atoms, O atoms in the oxide, and O atoms in H_2O molecules are plotted using black, red, and blue lines, respectively. The profiles for the different elements have been rescaled to fit on the same vertical scale.

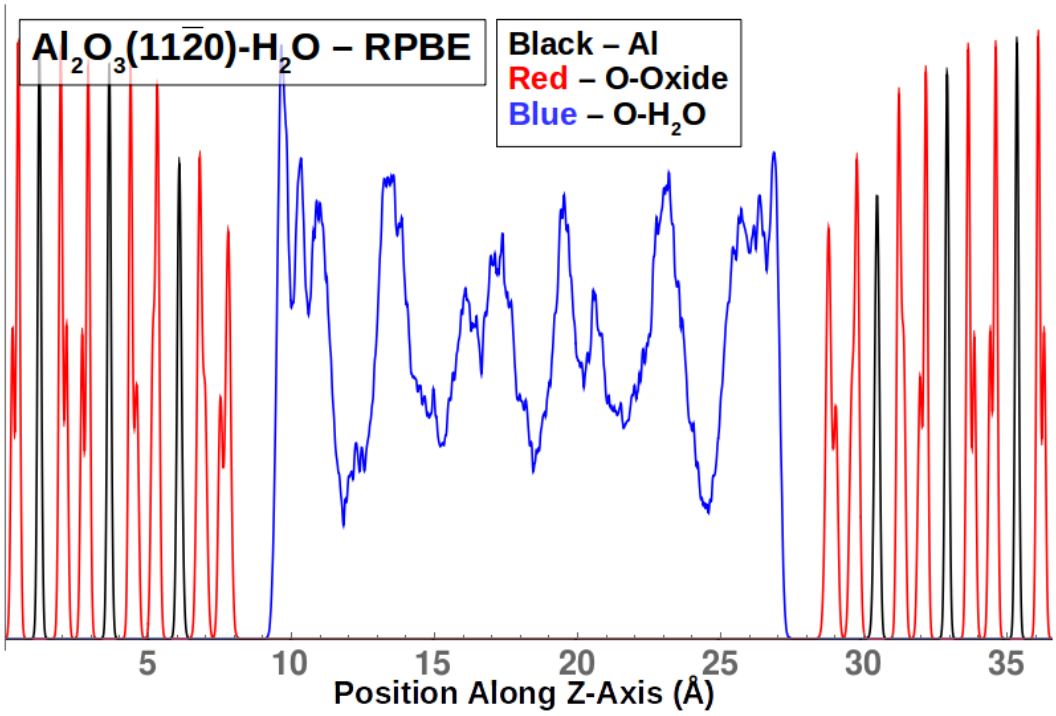

Figure 8: The density profile of the O and Al atoms for the (11$\bar{2}$0) interface simulated using the RPBE functional. The density profiles for the Al atoms, O atoms in the oxide, and O atoms in H_2O molecules are plotted using black, red, and blue lines, respectively. The profiles for the different elements have been rescaled to fit on the same vertical scale.

Vibrational Density of States of H_2O

In this section we plot the Vibrational Density of States (VDOS) of the H atoms which are part of H_2O molecules. We plot the VDOS for the (0001) interface in Figure 9 and we plot the VDOS for the $(11\bar{2}0)$ interface in Figure 10.

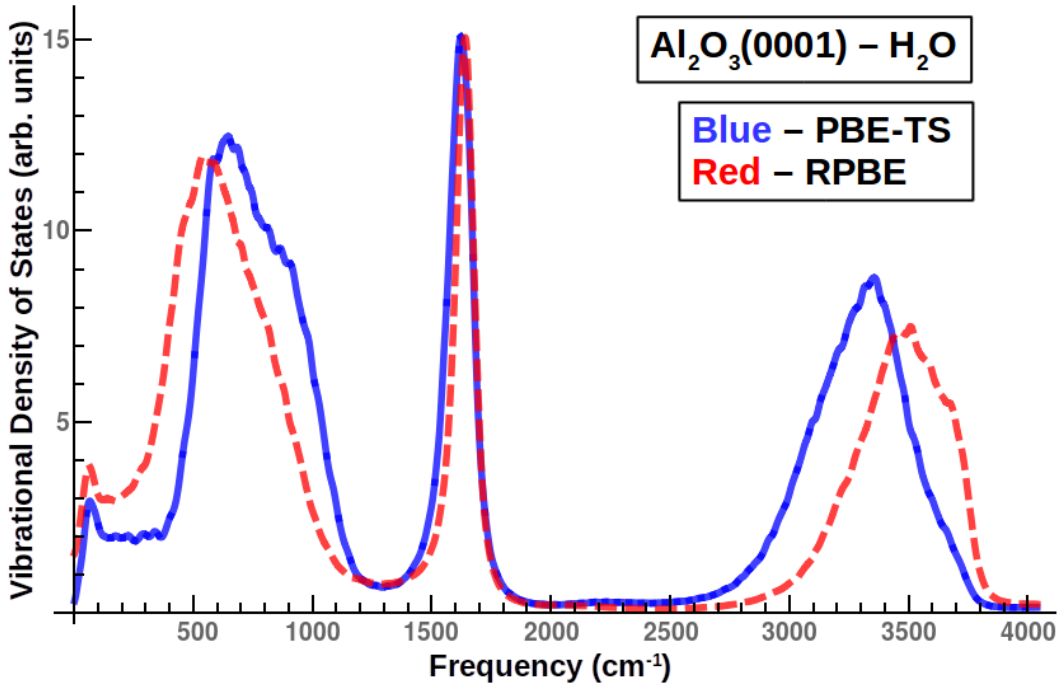

Figure 9: The VDOS of the H atoms which are part of H_2O molecules, averaged over all simulations of the Al_2O_3(0001)-H_2O interface. The blue solid line shows the VDOS for the PBE-TS simulations while the red dotted line shows the VDOS for the RPBE simulations.

Note that the RPBE functional results in an OH stretching peak in the VDOS with more weight at higher frequencies, even if we correct for the different location of the maxima of the two plots. This is more pronounced for the (0001) interface, with a noticeable difference in the shape of the OH-stretching peak. For both interfaces, if we red-shift the RPBE functional by 100 cm^{-1}, the maxima of the OH stretching peaks are aligned and there is strong overlap between the two peaks. Thus, in order to compare the SFG spectra obtained from the simulations using the two functionals, we will red-shift the RPBE spectra by 100 cm^{-1} such that the peaks of the two spectra should overlap.

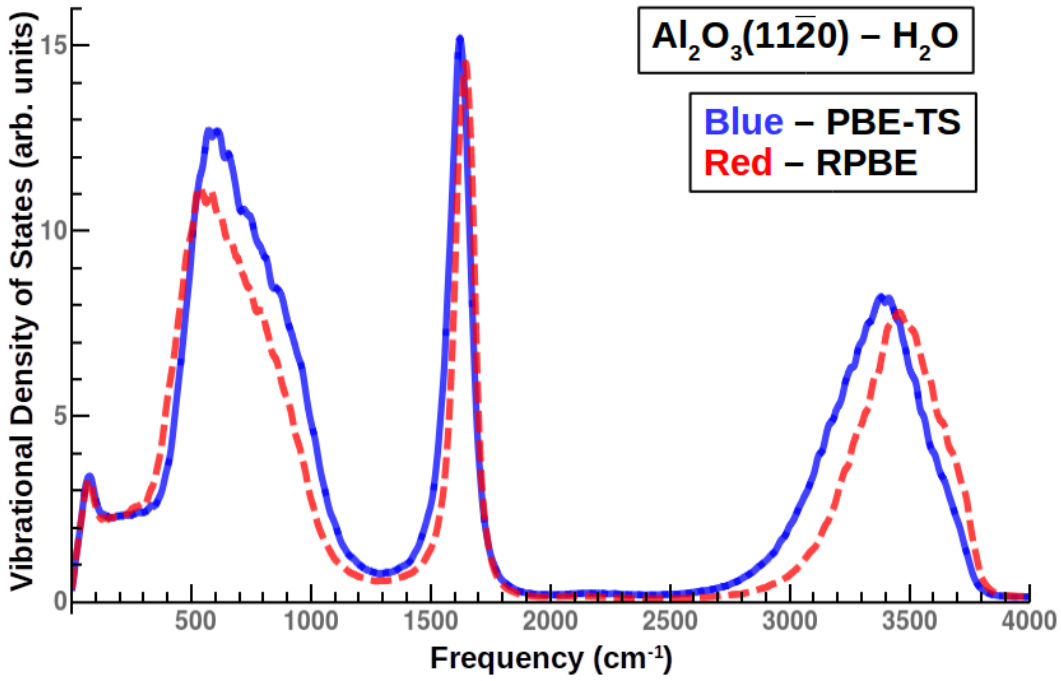

Figure 10: The VDOS of the H atoms which are part of H_2O molecules, averaged over all simulations of the Al_2O_3(0001)-H_2O interface. The blue solid line shows the VDOS for the PBE-TS simulations while the red dotted line shows the VDOS for the RPBE simulations.

vSFG Spectrum: PBE-TS Functional - No Filter

In this section, we plot the SFG spectrum of the (0001) and (11$\bar{2}$0) interfaces without using a Gaussian filter to smooth the spectra, in order to show the effect of the filter on the shape of the spectra. We plot the spectra for the (0001) and (11$\bar{2}$0) interfaces in Figures 11 and 12, respectively. Notice that there is a great deal of noise in the spectra, although the average shape still resembles the filtered spectra presented in the main manuscript. It is possible to smooth these spectra in the frequency domain by narrowing the time window used to remove edge effects in the Fourier transform. However, we chose not to do so as (1) we wanted to keep the desirable properties of the Blackman-Harris window[3] and its width is fixed to the size of the time interval, and (2) smoothing in the frequency domain allows for finer control of the smoothing process, allowing us to slowly decrease the resolution of the spectrum until the main features of the vSFG signal become clear.

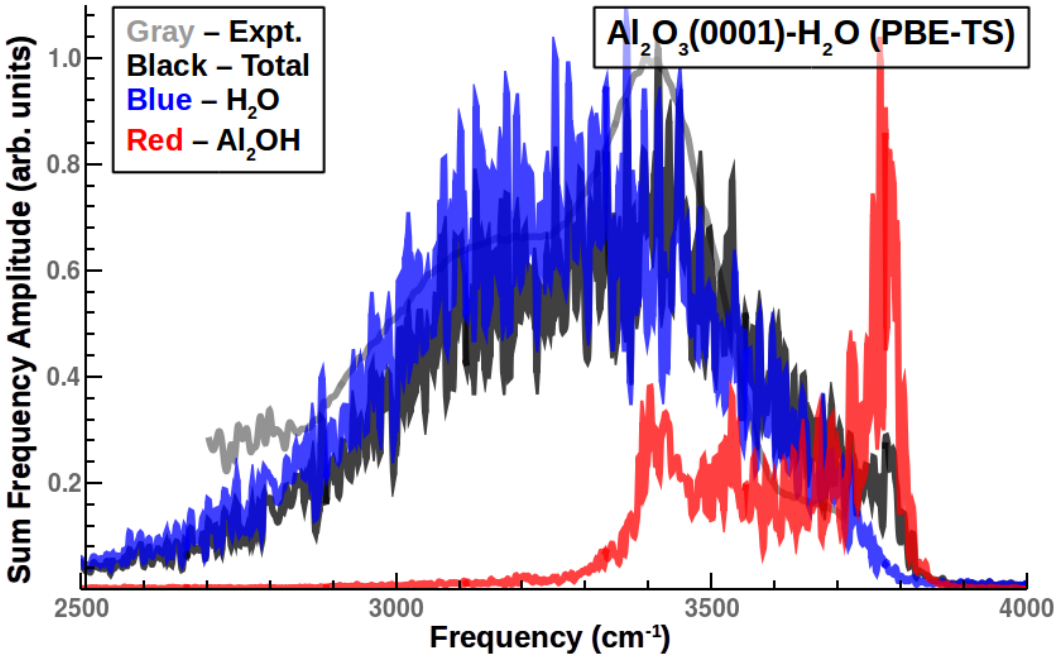

Figure 11: The SFG spectrum for the PPP polarization at the Al_2O_3(0001)-H_2O interface using the PBE-TS functional with no filtering of the final spectrum. The gray line is the experimental spectrum, the black line is the total calculated spectrum, the blue line is the spectrum calculated from only H_2O molecules, and the red line is the spectrum calculated only from surface OH groups. All experimental and calculated spectra have been normalized to their respective maxima in order to display them all on the same axes.

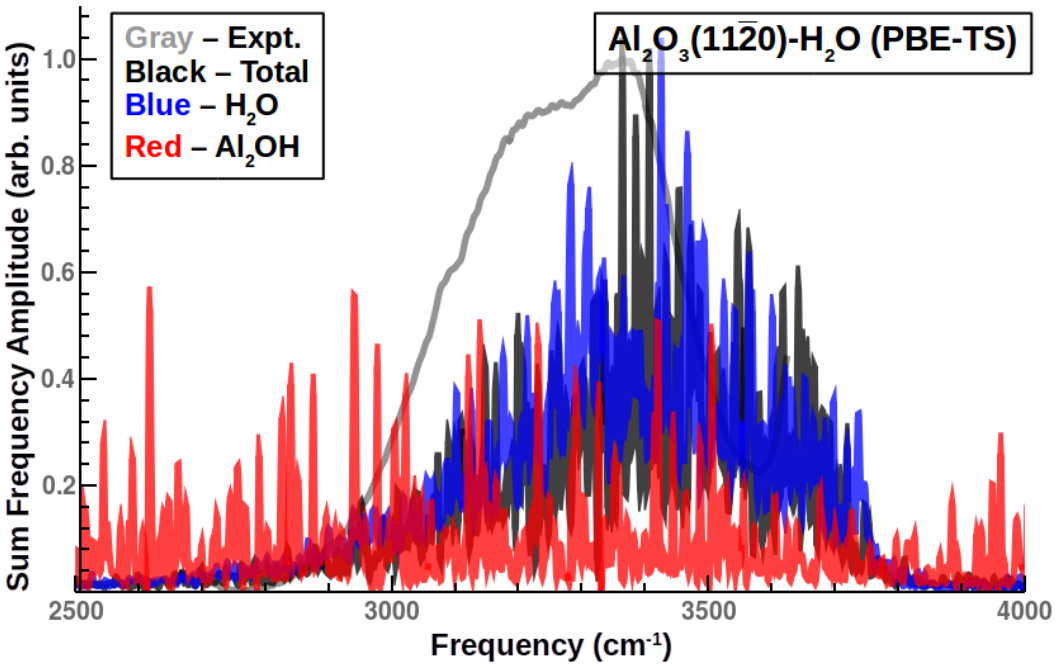

Figure 12: The SFG spectrum for the PPP polarization at the $Al_2O_3(11\bar{2}0)$-H_2O interface using the PBE-TS functional with no filtering of the final spectrum. The gray line is the experimental spectrum, the black line is the total calculated spectrum, the blue line is the spectrum calculated from only H_2O molecules, and the red line is the spectrum calculated only from surface OH groups. All experimental and calculated spectra have been normalized to their respective maxima in order to display them all on the same axes.

vSFG Spectrum: SSP

For comparison, we include here the SFG spectrum for the SSP polarization for each of the interfaces. We plot the SSP spectrum for the (0001) interface in Figure 13 and the SSP spectrum for the $(11\bar{2}0)$ in Figure 14. Note that the SSP spectra are similar to the PPP spectra, with the dominant frequencies still present in each, but with a different weighting of the dominant peaks in the spectrum.

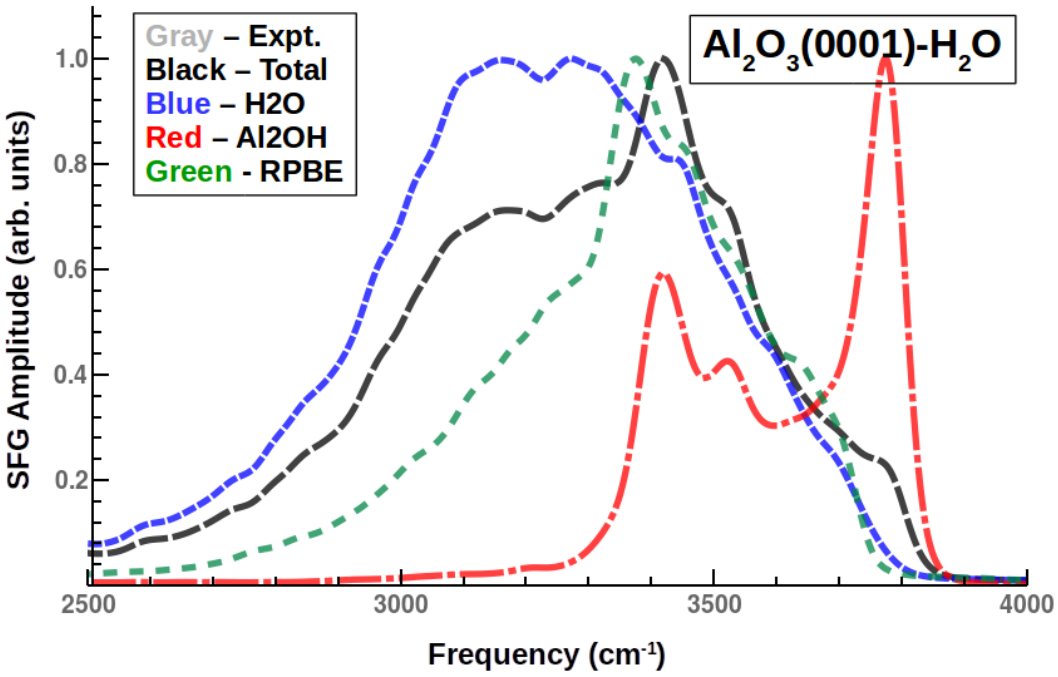

Figure 13: The vSFG spectrum for the SSP polarization at the Al_2O_3(0001)-H_2O interface. The black dashed line is the total calculated spectrum, the blue dotted line is the spectrum calculated from only H_2O molecules, the red dashed-dotted line is the spectrum calculated only from surface OH groups, and the green widely dotted line is the total calculated spectrum for the RPBE functional, red-shifted by 100 cm^{-1}. All calculated spectra have been normalized to their respective maxima in order to display them all on the same axes.

SFG - Correlation Cutoff Distance

Recall that the second order response function chi2 can be written as:

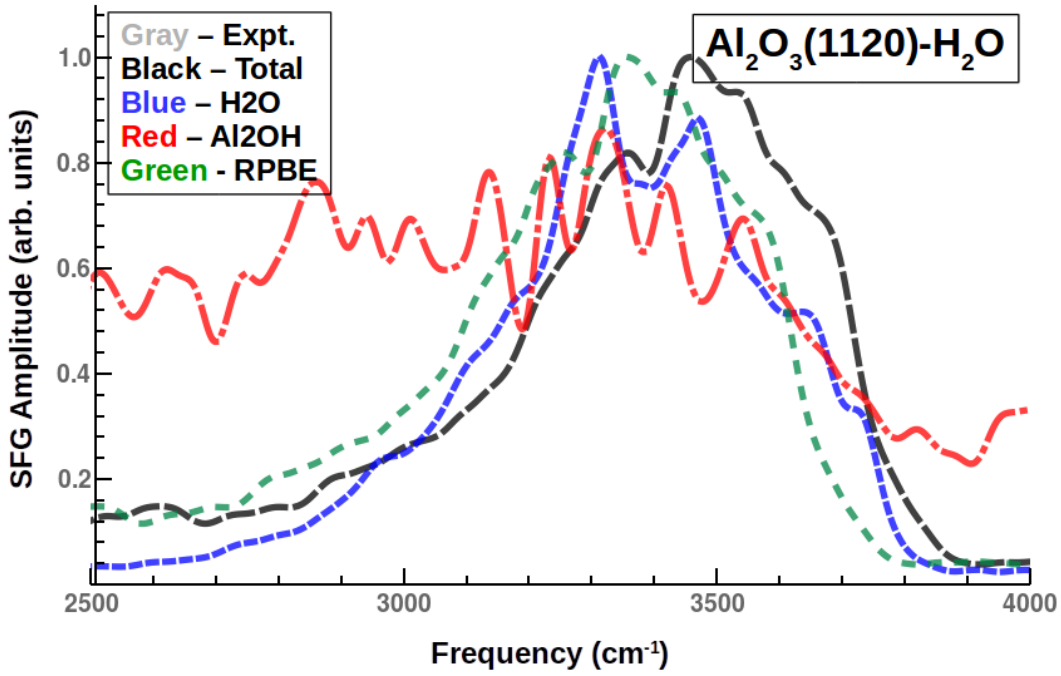

Figure 14: The vSFG spectrum for the SSP polarization at the $Al_2O_3(11\bar{2}0)$-H_2O interface. The black dashed line is the total calculated spectrum, the blue dotted line is the spectrum calculated from only H_2O molecules, the red dashed-dotted line is the spectrum calculated only from surface OH groups, and the green widely dotted line is the total calculated spectrum for the RPBE functional, red-shifted by 100 cm^{-1}. All calculated spectra have been normalized to their respective maxima in order to display them all on the same axes.

$$\chi^{(2)} = (i\omega kT)^{-1}\mathscr{F}[\langle\dot{\alpha}(t)\dot{\mu}(0)\rangle] \tag{1}$$

Since alpha and mu are the total polarizability and dipole moment of the system, we can write each as a sum over atomic or molecular polarizabilities, such that chi2 can be written as a sum of self- and cross-correlation terms:

$$\chi^{(2)} = (i\omega kT)^{-1}\mathscr{F}[\sum_i\langle\dot{\alpha}_i(t)\dot{\mu}_i(0)\rangle + \sum_{i\neq j}\langle\dot{\alpha}_i(t)\dot{\mu}_j(0)\rangle] \tag{2}$$

It is common practice in MD simulations to truncate the cross-correlation term, such that correlations of the polarizability and dipole moment between molecules is included only up to a certain cutoff distance. This is done because large CMD simulations over hundreds of ps shows that the cross-correlation terms can take tens to hundreds of ps to converge.

We chose not to truncate correlations in this work because of the small size of our simulation cell and because of the behavior of the SFG spectrum at the alumina-water interface with respect to the cutoff. Firstly, due to the limitations of DFT, we have relatively small simulation cells with roughly 1 nm^2 of water at each interface. We did investigate the behavior of the SFG spectrum with respect to the correlation cutoff however, and we found that a relatively large cutoff distance for the correlation cutoff is necessary for an accurate spectrum at the (001) interface. To illustrate this, we truncate the cross-correlation terms by multiplying them by a Fermi-type cutoff of the bond-bond distance dr: $F_{cut}(dr) = 1.0/(1.0 + \exp((dr - R)/D))$ where R is the cutoff distance and D is the width of the cutoff. We plot the SFG spectrum for the PBE-TS functional with respect to cutoff distance for the (0001) interface in Figure 15 and for the $(11\bar{2}0)$ interface in Figure 16.

While the SFG spectrum does not change much with respect to cutoff distance for the $(11\bar{2}0)$ interface, we find that there are significant differences for the (0001) interface. Namely, for very small cutoffs (1 Å), we see a prominent peak at ∼3700 cm^{-1}, reducing in intensity as the cutoff distance is increased. This peak is contributed almost entirely from the out-of-

plane aluminols at the (0001) surface. This peak is largest for small cutoffs because, without considering correlations, the SFG intensity should be proportional to the orientational average of a molecule over the lifetime of a simulation. Since the aluminols are fixed to the surface with relatively stable orientations compared to the H2O molecules, we expect them to have greater intensity with small correlation cutoffs. As the cutoff is increased, the 3700 cm^{-1} peak decreases in intensity as almost all cross-correlation terms at that frequency are zero as the out-of-plane aluminol is the minority vibrational chromophore. Thus, because of the insensitivity of the cutoff on the spectrum at the $(11\bar{2}0)$ interface and because of the effect of the cutoff on the surface modes at the (0001) interface, we believe not truncating the correlation function in our simulations yields an accurate SFG spectrum.

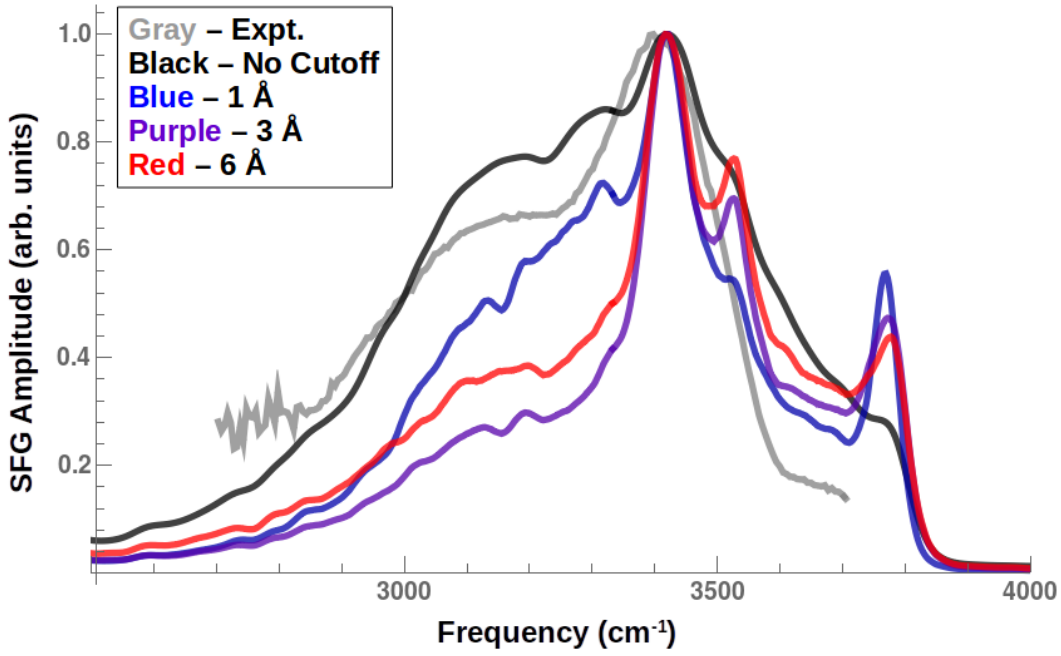

Figure 15: The SFG spectrum for PPP polarization as a function of cutoff distance at the alumina(0001)-H_2O interface. The gray line is the experimental spectrum, the black line is for no cutoff, and the blue, red, and purple lines are for cutoff of 1, 3, and 6 Å with a width of 0.5 Å.

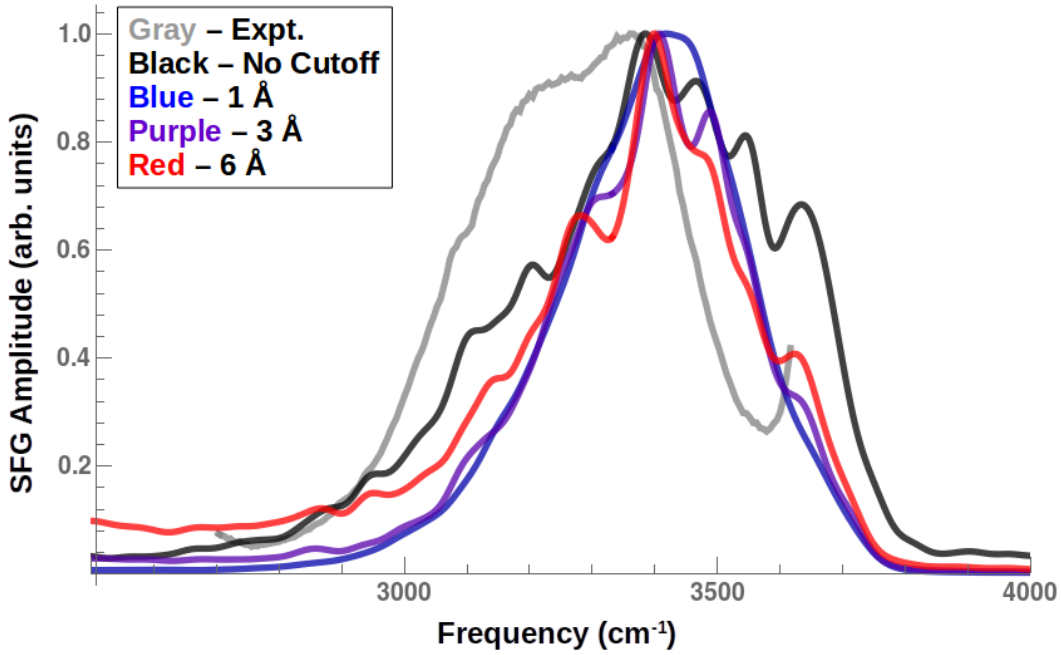

Figure 16: The SFG spectrum for PPP polarization as a function of cutoff distance at the alumina($11\bar{2}$)-H_2O interface. The gray line is the experimental spectrum, the black line is for no cutoff, and the blue, red, and purple lines are for cutoff of 1, 3, and 6 Å with a width of 0.5 Å.

Dependence of SFG on Bond Position

Because of small but non-negligible contributions to the SFG spectrum from the electric quadrupole and magnetic dipole, there exist ambiguities in the SFG spectrum and how one separates the two interfaces present in a period MD simulation1. Namely, the position of the molecule or bond used to determine which half of the cell it is in can impact the shape of the spectrum2. In the main manuscript we set the positions of O-H bonds to halfway between O and H atoms, but setting the position to 15% along the O-H bond near the O atom has been shown to reduce higher order contributions to the SFG spectrum, thereby improving the accuracy of the dipole approximation. We plot the SFG spectrum for both bond position definitions for the (0001) interface in Figure 8 and we see that there is very little difference between the two spectra, except for slightly more noise for the 15% bond position. Thus, for the alumina-water system we find there is little dependence of the SFG spectrum on the definition for the bond position.

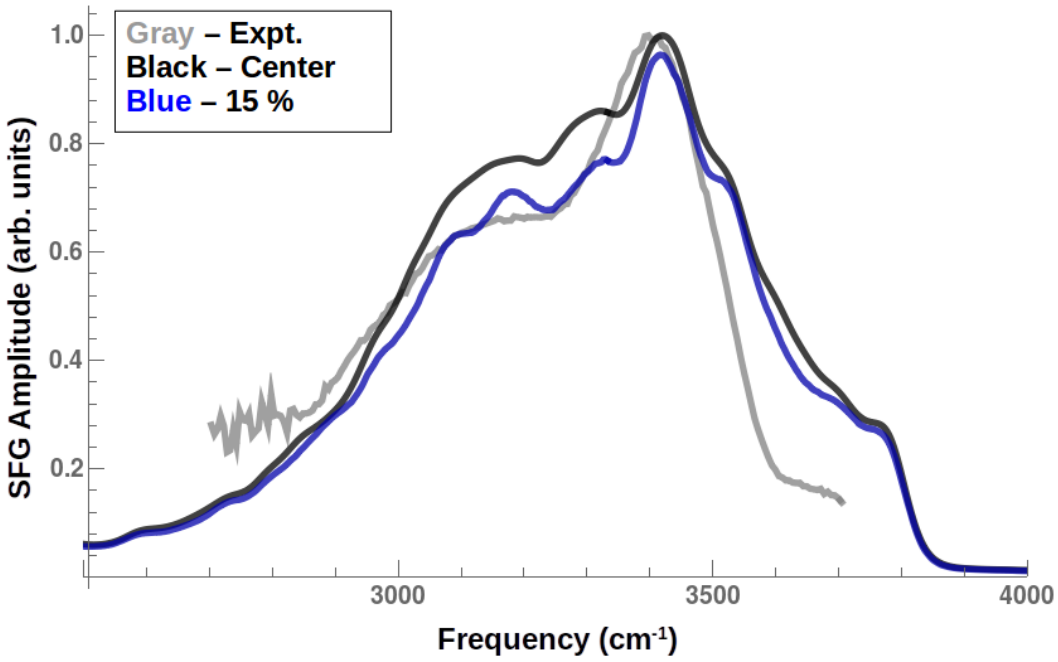

Figure 17: The SFG spectrum for PPP polarization at the alumina(0001)-H_2O interface for two different bond position definitions. The gray line is the experimental spectrum, the black line shows the SFG spectrum where the bond position at the midpoint between the O and H atoms while the blue line shows the SFG spectrum where the bond position is 15% along the O-H bond from the O position.

SFG Calculation

In this section we review our methodology for calculation of the SFG spectrum in greater detail. The first step is to calculate the dipole moments and polarizabilities of the bonds in the simulation. As stated in the main text, we begin by assigning each atom a gas-phase polarizability, which is a parameter for each element determined by a fit to a large database of molecular polarizabilities. We then calculate the dipole interactions between each atom using Thole's damped dipole interaction derived from a H-atom-like charge density:

$$T_{ij} = \delta_{ij}/r^3(1-((ar)^2/2+ar+a)e^{-ar}) - r_i r_j/r^5(1-((ar)^3/6+(ar)^2/2+(ar)+1)e^{-ar}) \quad (3)$$

moments and polarizabilities of the bonds in the simulation. Using Tholes method,[4,5] we are able to calculate effective polarizabilities α_i^{eff} for each atom i such that the total polarizability of the system is a sum over the polarizabilities of each atom. Because of the additivity of the polarizabilities, we are free to define the bond polarizability as a sum over the polarizabilities of the two atoms in the bond, where we first divide each atomic polarizabilitity by the number of bonds of each atom. The resulting bond polarizabilities then sum to the total polarizability of the system and we have found them to be a good approximation of the polarizability of the molecules.[6]

Once we have obtained the bond polarizabilities we then calculate self-consistent bond dipoles using these polarizabilities, starting with nominal dipole moments calculated from simple atomic charges, in this case take from the ClayFF force field.[7]

Once the dipole moments and polarizabilities are obtained, we then calculate the Fourier transform of the correlation function $\langle\alpha(t)\mu(0)\rangle$. We first calculate the Fourier transforms of each, namely $\tilde{\alpha}(\omega)$ and $\tilde{\mu}(\omega)$, making sure to pad each with zeros such that we double the total length of each. Note that the padding is required to prevent spurious correlations. We then multiply $\tilde{\alpha}$ and $\tilde{\mu}$ at each frequency to get the correlation function in the frequency

domain and take the inverse Fourier transform to obtain the correlation function in the time domain. Finally, we apply a Blackman-Harris window[3] to the correlation function and take the Fourier transform again to get the windowed correlation function in the frequency domain.

Once we have obtained $\chi^{(2)}$, which is directly available from the Fourier transform of the correlation function $\langle \alpha(t)\mu(0) \rangle$, we can then calculate the SFG spectrum. Recall that the SFG intensity can be obtained by $\chi^{(2)}$ using the equation:

$$I(\Omega) = 8\pi^3\Omega^2 \sec^2(\theta)/(c^3[\epsilon(\Omega)\epsilon(\omega_V)\epsilon(\omega_{IR})]^{1/2})|e_I(\Omega)\chi^{(2)}(\Omega)e_J(\omega_V)e_K(\omega_{IR})|I(\omega_{IR})I(\omega_V) \tag{4}$$

which we discuss in the main text. In order to calculate the PPP spectrum we take the polarization vectors e to be the following:

$$e = (\sin(\theta)\cos(\phi), \sin(\theta)\sin(\phi), \cos(\theta)) \tag{5}$$

where phi is the polar angle and theta is the angle the electric field component of the incoming radiation makes with the surface normal (i.e. the complement of the laser propagation direction). Each polarization vector is obtained from the experimental laser geometry for the IR and VIS lasers, and the SFG polarization vector is obtained using the nonlinear generalization of Snells law.[8] Finally, once theta is obtained for each laser, we average the intensity over the polar angle ϕ (note: there is very little dependence of the spectrum on ϕ).

Polarizability Parameters

As mentioned above, we use a Thole-type model[4,5] to calculate the polarizability for all the bonds in the system. This model includes short-range corrected dipole interactions to calculate effective, additive atomic polarizabilities from initial gas-phase atomic polarizabilities.

The parameters for this model are a distance scaling parameter a and the gas-phase polarizabilities for each element in the system. We fit these parameters to DFT polarizabilities of the H_2O molecule for 576 configurations and the ground state configuration for the $Al(OH)_3$ molecule. We calculate the polarizabilities of the molecules using the ωB97XD[9] functional and the dAug-cc-pVTZ[10,11] basis set as implemented in Gaussian09. The parameters for the Thole model are presented in Table 3.

Table 3: Table 1: Parameters for Thole Polarizability Model

Parameter	Value
a	1.96069
$\alpha_H^{(0)}$	0.34 Å^3
$\alpha_O^{(0)}$	1.40 Å^3
$\alpha_{Al}^{(0)}$	1.65 Å^3

We present the results of the fit for the H_2O molecules in Figure 18, comparing the Thole polarizabilities to the ab-initio polarizabilities. We see that, while the Thole model underestimates the magnitude of the change of the polarizability with changes in the O-H bond distance, it does reproduce the qualitative dependence of the polarizability on the molecular coordinates. Since we are concerned primarily with the relative magnitudes of the polarizabilities of the O-H bonds in the system and their frequency dependence in the O-H stretching region, we are confident in using this model to calculate the SFG spectrum of the Al_2O_3(001)-H_2O interface.

Real and Imaginary Part of $\chi^{(2)}$

The real an imaginary part of $\chi^{(2)}$ are plotted in Figure 19 for the PBE-TS functional for the (0001) alumina-water interface, averaged over each simulation and interface. Note that the imaginary part is large and negative around 3200 cm^{-1}, associated with H_2O molecules with OH groups pointing down towards the interface, before increasing to zero around 3400 cm^{-1} as the surface aluminols, which point slightly out of the interface, and H_2O molecules

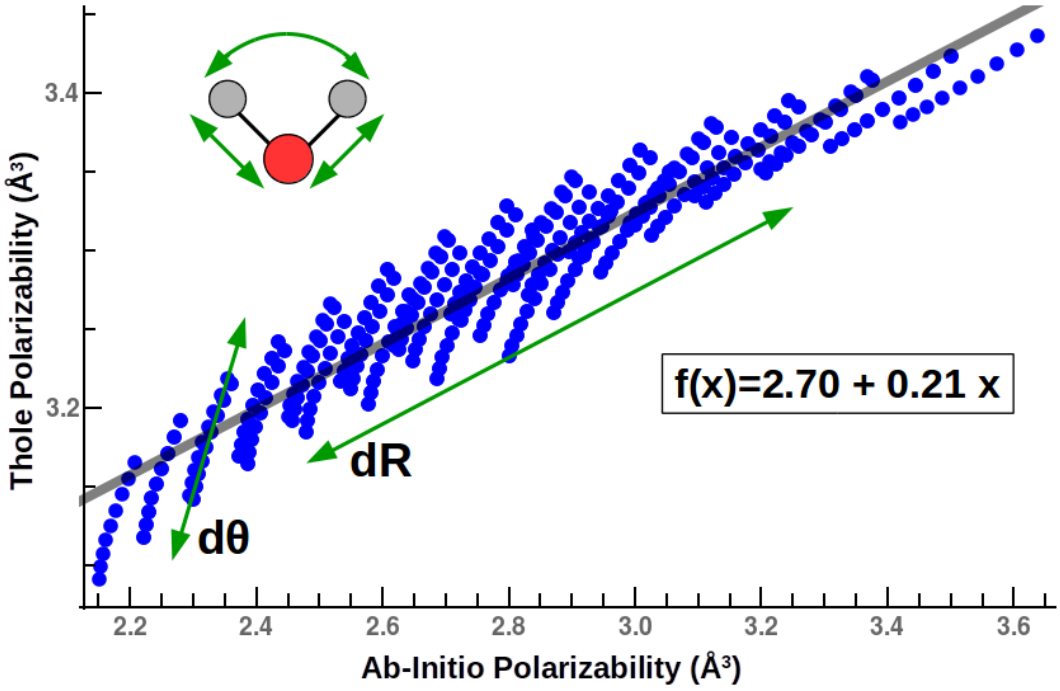

Figure 18: Plot of the ab-initio vs. Thole polarizability of a H_2O molecule for 576 different configurations obtained by varying the H-O-H angle and two O-H bonds. The line is a linear fit to the data, with the function shown in the plot.

with relatively weak H-bonds to other H_2O molecules begin to contribute to the 3400 cm^{-1}.

Sample Preparation

α-Al_2O_3(0001) cut equilateral roof prisms (15 x 13 x 13 x 15 mm) purchased from Team Photon Inc. (San Diego, CA) served as the alumina surface for our experiments. The 15 x 15 mm^2 surface (opposite of roof) was the sampling area. Prisms were first cleaned with "piranha" solution (1 vol. conc. H_2O_2: 3 vol. conc. H_2SO_4) for ~30 min in a Teflon container. (CAUTION: *piranha is extremely reactive and can cause severe damage to skin/eyes. Handle using gloves, goggles, lab coat, and extreme care.*) To remove any remaining piranha solution they were then rinsed with copious amounts of deionized water (>18.2 MΩ cm resistivity, Thermoscientific Barnstead Easypure II purification system with UV lamp) and dried using high purity N_2 gas. Lastly, the sample holder, a Teflon o-ring,

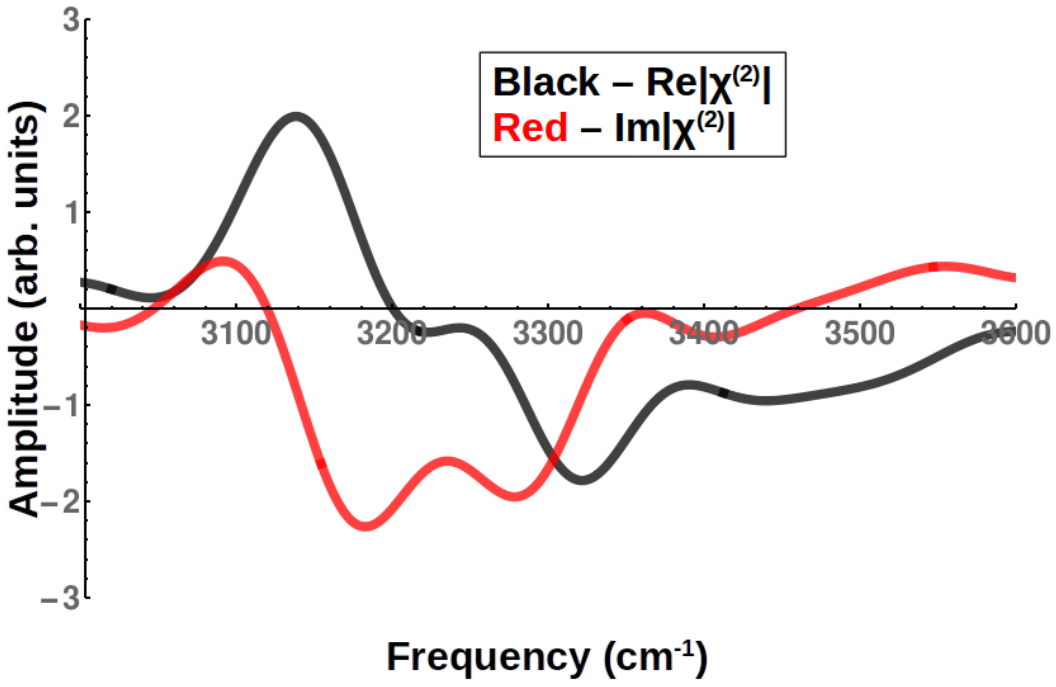

Figure 19: The real an imaginary part of $\chi^{(2)}$ for the PBE-TS functional for the (0001) alumina-water interface.

and prism itself are cleaned using low-pressure RF plasma for ∼30 min. Prisms are allowed to equilibrate to room temp under vacuum and are exposed to water for ∼15 minutes before experiments are performed. The prisms are mounted in a sample holder with flow through ports and one prism was coated with a ∼100 nm film of Au for use as a nonresonant reference to measure IR pulse profiles.

References

(1) Catalano, J. G. Weak interfacial water ordering on isostructural hematite and corundum (001) surfaces. *Geochimica et Cosmochimica Acta* **2011**, *75*, 2062–2071.

(2) Catalano, J. G. Relaxations and Interfacial Water Ordering at the Corundum (110) Surface. *The Journal of Physical Chemistry C* **2010**, *114*, 6624–6630.

(3) Harris, F. J. On the use of windows for harmonic analysis with the discrete Fourier transform. *Proceedings of the IEEE* **1978**, *66*, 51–83.

(4) Applequist, J.; Carl, J. R.; Fung, K.-K. Atom dipole interaction model for molecular polarizability. Application to polyatomic molecules and determination of atom polarizabilities. *Journal of the American Chemical Society* **1972**, *94*, 2952–2960.

(5) Thole, B. Molecular polarizabilities calculated with a modified dipole interaction. *Chemical Physics* **1981**, *59*, 341–350.

(6) DelloStritto, M.; Sofo, J. Bond Polarizability Model for Sum Frequency Generation at the $Al_2O_3(0001)H_2O$ Interface. *The Journal of Physical Chemistry A* **2017**, *121*, 3045–3055.

(7) Cygan, R. T.; Liang, J.-J.; Kalinichev, A. G. Molecular Models of Hydroxide, Oxyhydroxide, and Clay Phases and the Development of a General Force Field. *The Journal of Physical Chemistry B* **2004**, *108*, 1255–1266.

(8) Bloembergen, N.; Pershan, P. S. Light Waves at the Boundary of Nonlinear Media. *Physical Review* **1962**, *128*, 606–622.

(9) Chai, J.-D.; Head-Gordon, M. Long-range corrected hybrid density functionals with damped atomatom dispersion corrections. *Physical Chemistry Chemical Physics* **2008**, *10*, 6615–6620.

(10) Kendall, R. A.; Jr, T. H. D.; Harrison, R. J. Electron affinities of the firstrow atoms revisited. Systematic basis sets and wave functions. *The Journal of Chemical Physics* **1992**, *96*, 6796–6806.

(11) Dunning, T. H. Gaussian basis sets for use in correlated molecular calculations. I. The atoms boron through neon and hydrogen. *The Journal of Chemical Physics* **1989**, *90*, 1007–1023.